JOURNAL OF SOLID STATE CHEMISTRY 87, 55–63 (1990)

Oxidation–Reduction Behavior of Undoped and Sr-Doped $LaMnO_3$: Defect Structure, Electrical Conductivity, and Thermoelectric Power

J. H. KUO AND H. U. ANDERSON

Ceramic Engineering Department, University of Missouri–Rolla, Rolla, Missouri 65401

AND D. M. SPARLIN

Physics Department, University of Missouri–Rolla, Rolla, Missouri 65401

Received June 22, 1989; in revised form March 12, 1990

Seebeck coefficient and electrical conductivity measurements were performed for undoped and Sr-doped $LaMnO_3$ as a function of temperature and oxygen partial pressure. The results of electrical conductivity showed typical *p*-type behavior. As reduction proceeded, the electrical conductivity of these $LaMnO_3$-based perovskites decreased with $P_{O_2}^{1/4}$. The analysis of the electrical conductivity data was performed by extending the defect model from a previous thermogravimetric (TG) study. The measured Seebeck coefficients were found to be positive except for the most reducing conditions when the decomposition into multiple phases occurred. The Heikes formula was adopted to interpret the Seebeck coefficient results and to calculate the mobility. These results indicated that the conduction was due to *p*-type carriers of a localized nature. It was also suggested that the conductivity for these perovskites was dominated by the mobility rather than by the carrier concentration.

1. Introduction

The $LaMnO_3$ based perovskites are nonstoichiometric oxides which are currently being used as air electrodes in high temperature solid state fuel cells. Defect structures and thermodynamic properties for both undoped and Sr-doped $LaMnO_3$ determined from thermogravimetric data were previously reported (*1*). In the present study, both the electrical conductivity and the Seebeck coefficient were determined as a function of oxygen partial pressure and temperature. The electrical conductivity data were analyzed by using the defect structure obtained from the previous thermogravimetric study. Carrier concentration and mobility were determined by the dc electrical conductivity and Seebeck coefficient data. Activation energies were also calculated from electrical conductivity, Seebeck coefficient, and mobility data, respectively.

2. Experimental

Undoped and Sr-doped $LaMnO_3$ powders were prepared by a liquid mix method similar to that first described by Pechini (*3*). For all calcined compositions, X-ray diffraction analysis showed a perovskite structure. No additional phases were detected.

Rectangular-shaped specimens were prepared by dry pressing powder at 300 kg/cm^2 and sintering at 1450°C for 2 days in air. The densities of the sintered bars were greater than 90% of theoretical. The electrical con-

0022-4596/90 $3.00

ductivity was measured as a function of oxygen activity by using a four-probe technique (*4*). A Hewlett–Packard 651B test oscillator was used to supply the current while the output voltage was measured by using a PAR 186 lock-in amplifier. In order to eliminate the 60-Hz inductive noise a test frequency of 400 Hz was used in the measurement. The accuracy of the electrical conductivity measurement was determined to be within $\pm 1\ (\Omega\text{-cm})^{-1}$. Oxygen activity control was achieved with flowing gas mixtures composed of either O_2–N_2 or CO_2-forming gas (10% H_2–90% N_2). A stabilized zirconia oxygen sensor was used to monitor the oxygen partial pressure (P_{O_2}) of the gas mixture. In a separate apparatus, the Seebeck coefficient and dc electrical conductivity were sequentially measured on the same specimen. The specimen was situated between two Pt blocks. Two Pt (Pt–10% Rh) thermocouples were used to monitor the temperatures at the ends of the specimen. A Pt wire heater was wound on the lower end of the holder to generate a temperature gradient along the longitudinal direction. The P_{O_2} control was achieved by mixing the gas species in a desired ratio through a set of electronic mass flow controllers. The gas flow rate was controlled to ± 0.01 cm^3/min. Seebeck coefficients were determined by measuring temperature gradients and thermal emf's through the common leads of the thermocouples. The dc electrical conductivity measurements were made by using the Kelvin technique in which two leads carry the sample current (1 mA) and the other two measure the voltage drop. These measurements gave identical results to those from the four-probe, 400-Hz method.

3. Results and Conclusion

A. Electrical Conductivity

The ac (400 Hz) electrical conductivity measurements showed that both undoped and Sr-doped $LaMnO_3$ had similar oxidation–reduction behavior. The electrical conductivity was nearly constant in the high P_{O_2} range within experimental error. As reduction progressed, the conductivity decreased as a function of P_{O_2} to the one-quarter power.

The constant electrical conductivity which exists in the high P_{O_2} region may be easily understood if it is assumed that acceptors control the carrier concentration and that electronic compensation predominates. In the lower P_{O_2} region, oxygen vacancies are formed and the electrical conductivity begins to decrease due to ionic charge compensation.

Since this is similar behavior to that which has been observed for Mg-doped $LaCrO_3$ (*5*), analogous modeling has been adopted.

(*1*) *Sr-Doped LaMnO$_3$*

For the oxygen-deficient region the same defect reaction applies as was developed for the thermogravimetric measurements (*1*). As was shown the defect reaction may be represented by

$$La_{1-x}Sr'_yMn^x_{1-y}Mn^{\cdot}_yO_3 \rightleftharpoons La_{1-y}Sr'_yMn^x_{1-y+2x}Mn^{\cdot}_{y-2x}V^{\cdot\cdot}_{O_x}O_{3-x} + x/2\ O_2, \quad (1)$$

where y represents the dopant concentration and x, the oxygen vacancy, or

$$2Mn^{\cdot}_{Mn} + O_0 \rightleftharpoons 2Mn^x_{Mn} + V^{\cdot\cdot}_0 + \tfrac{1}{2}O_2. \quad (2)$$

The equilibrium constant is given by

$$K_1 = [Mn^x_{Mn}]^2[V^{\cdot\cdot}_0]P^{1/2}_{O_2}/[Mn^{\cdot}_{Mn}]^2[O_0], \quad (3)$$

which after substitution in terms of mole fraction becomes

$$K_1 = (1 - y + 2x)^2(x)P^{1/2}_{O_2}/\{(y - 2x)^2(3 - x)\}. \quad (4)$$

With little loss in precision, this expression can be approximated as

$$K_1 = xP^{1/2}_{O_2}/(y - 2x)^2. \quad (5)$$

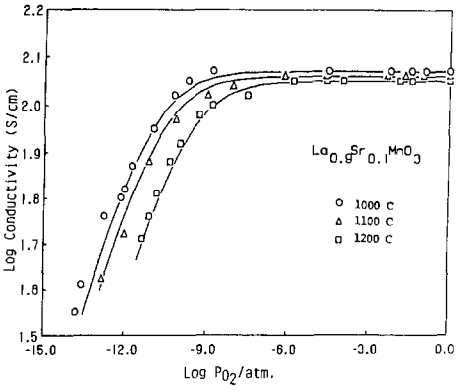

FIG. 1. Log conductivity (400 Hz) vs log P_{O_2} for $La_{.90}Sr_{.10}MnO_3$ at various temperatures. The solid lines are calculated.

The electrical conductivity is given by $\sigma = e\mu p$, where e is the magnitude of the charge on a single hole, μ is the mobility, and p is the hole concentration. In the low P_{O_2} region, the carrier concentration is given by $p = y - 2x$. In this region, when the carrier concentration is combined with Eq. (5), the electrical conductivity is given by

$$\sigma = (e\mu/4K_1)P_{O_2}^{1/2}[(8yK_1P_{O_2}^{-1/2} + 1)^{1/2} - 1]. \quad (6)$$

At the higher P_{O_2} limit (x approaches zero), Eq. (6) reduces to $\sigma = e\mu p$. However, at low P_{O_2},

$$p = (y/2K_1)^{1/2}P_{O_2}^{1/4}, \quad (7)$$

and the conductivity becomes

$$\sigma = e\mu(y/2K_1)^{1/2}P_{O_2}^{1/4}. \quad (8)$$

By assuming that the mobility is a constant at a given temperature, the relative electrical conductivity σ_R can be expressed by

$$\sigma/\sigma_R = P_{O_2}^{1/4}/(2K_1y)^{1/2}, \quad (9)$$

where σ_R is the conductivity at 1 atm P_{O_2}.

The equilibrium constant K_1 can be found by combining the electrical conductivity data and Eq. (8). The theoretical curves can be generated by using Eq. (8) and the calculated values of K_1.

The results of the ac conductivity measurements made as a function of temperature for both 10 mol% and 20 mol% Sr-doped $LaMnO_3$ are shown in Figs. 1 and 2, respectively. The individual symbols represent the experimental data while the lines are the calculated curves.

(2) *Undoped $LaMnO_3$*

Previous TG results (*1*) found that undoped $LaMnO_3$ maintained a molar oxygen content equal to 2.999 over the stable P_{O_2} range. The presence of 0.1 mol% oxygen vacancies is of no consequence in samples doped with 10% Sr, since the effective acceptor level is then 9.9% rather than 10%. The conductivity of the undoped $LaMnO_3$ has fewer small polarons, however, and the oxygen vacancies compensate a significant fraction of those present. Assuming comparable mobilities, the nominal carrier concentrations of the doped and undoped $LaMnO_3$ samples were in accord with the doping level when 0.1% oxygen vacancies were assumed. The results obtained for electrical conductivity measurements of undoped $LaMnO_3$ performed at different tempera-

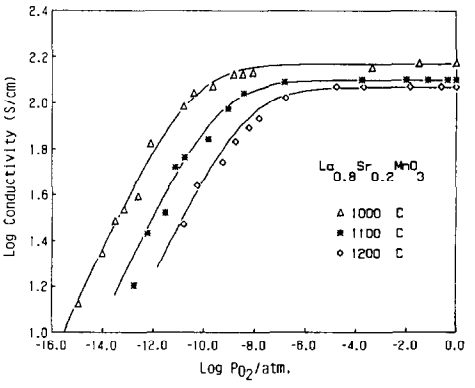

FIG. 2. Log conductivity (400 Hz) vs log P_{O_2} for $La_{.80}Sr_{.20}MnO_3$ at various temperatures. The solid lines are calculated.

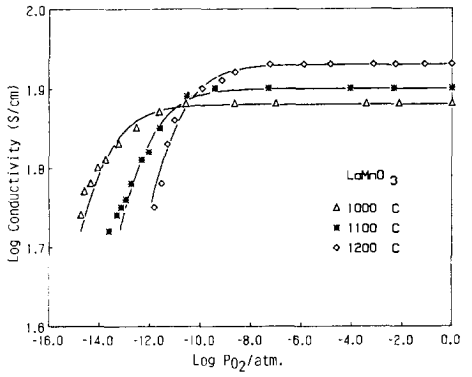

FIG. 3. Log conductivity (400 Hz) vs log P_{O_2} for $LaMnO_3$ at various temperatures. The solid lines are calculated from the model and by assuming 0.2 mol% Sr content.

tures are shown in Fig. 3. Typical results for the effects of Sr content on conductivity are presented in Fig. 4.

Both undoped and Sr-doped $LaMnO_3$ showed common characteristics:

(i) Little P_{O_2} dependence was observed in a range of high P_{O_2}, and this range narrows with increasing temperature.

(ii) As reduction proceeded, the electrical conductivity decreased with $P_{O_2}^{1/4}$ which agrees well with Eq. (8).

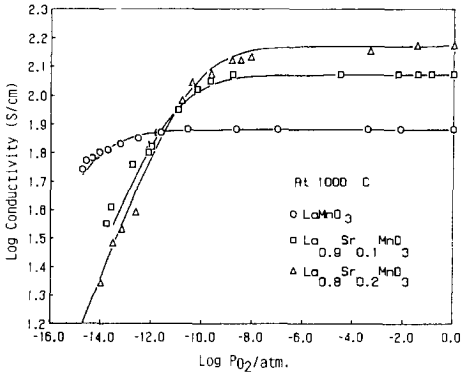

FIG. 4. Log conductivity (400 Hz) vs log P_{O_2} for various Sr-dopant levels at 1000°C. The solid lines are calculated.

(iii) An abrupt decrease of the electrical conductivity occurred under very reducing conditions. These conductivities were too low to be included in Figs. 1 to 4. However, by comparing with the previous TG data, it was found that the abrupt decrease in electrical conductivity was due to the decomposition of the perovskite phase. For each isotherm shown in Figs. 1 to 4, the symbol at the lowest P_{O_2} value indicates the "critical P_{O_2}" point, i.e., the lowest P_{O_2} before the oxide dissociated into multiple phases. Very good reversibility was found upon reoxidation.

(iv) The critical P_{O_2} shifted to higher P_{O_2} when the temperature and/or the dopant concentration was increased.

(3) *Temperature Dependence*

The equilibrium constants K_1 for undoped and Sr-doped $LaMnO_3$ calculated from the above conductivity analysis are listed in Table I along with those obtained from a previous TG study. Although these two studies adopted an identical expression for the equilibrium constant K_1, the equilibrium constants calculated from the electrical conductivity data were higher than those from the TG results. Note that the K_1 values reported in this paper are calculated from Eq. (9) in which the mobility was assumed to be a

TABLE I

LIST OF THE EQUILIBRIUM CONSTANTS K_1 AND K_9

Compound	1000°C	1100°C	1200°C
	Log equilibrium constant		
Undoped $LaMnO_3$	−5.15	−4.30	−3.69
	(−7.40)[a]	(−6.32)	(−5.38)
$La_{.90}Sr_{.10}MnO_3$	−5.15	−5.00	−4.52
	(−8.04)	(−6.95)	(−6.01)
$La_{.80}Sr_{.20}MnO_3$	−5.04	−4.52	−4.00
	(−8.68)	(−7.59)	(−6.65)

[a] Values in parentheses were obtained from thermogravimetric data (*1*).

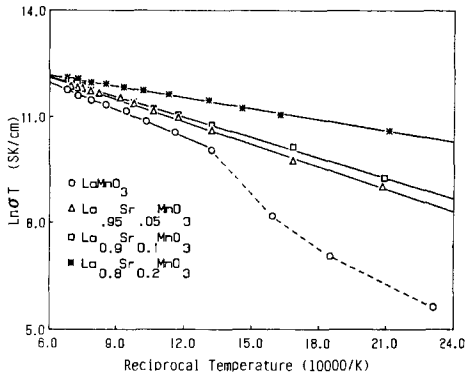

FIG. 5. Ln σ T (400 Hz) vs reciprocal temperature for undoped and Sr-doped $LaMnO_3$. Ln is the natural logarithm. The solid lines are calculated by the least-squares method.

constant. As will be shown, when the estimated mobility values, which showed a strong P_{O_2} dependence, were used to reevaluate the equilibrium constants, a better agreement between K_1 calculated from electrical conductivity and that from the TG results was found.

The ac electrical conductivity of undoped $LaMnO_3$ was measured in oxygen over the temperature range 150 to 1000°C. The results are shown in Fig. 5 in which a transition point was found around 660 K. Similar observations were reported previously (*6*) and may be explained by a orthorhombic–rhombohedral crystallographic transition (*7*). It was found that the electrical conductivity of undoped $LaMnO_3$ displayed the temperature dependence of a semiconductor. The linear relationship between $\ln(\sigma T)$ and $1/T$ above the transition temperature indicates that the conduction may be due to the small polaron mechanism.

Similar experiments were made on $LaMnO_3$ containing up to 20 mol% Sr with the results shown in Fig. 5. When the temperature was below 1000°C, the electric conductivity increased rapidly with increasing temperature. For temperature above 1000°C, the conductivity became nearly constant with temperature. However, as can be seen in Figs. 1 to 3, the electrical conductivity shows a transition from positive to negative temperature dependence as the Sr content is increased to 20%. This suggests a semiconducting to metallic transition. According to the previous studies for $LaCoO_3$ (*8*), such a semiconducting metallic transition may be due to a localized to collective electron transition. Similar results were also found for other La-site-substituted lanthanum manganites of the type $La_{1-x}M_xMnO_3$ (M = Pb^{+2}, Ba^{+2}, Ca^{+2}) (*9, 10*).

At temperatures below 1000°, the activation energies were determined by using the expression derived for the small polaron mechanism,

$$\sigma = (A/T)\exp(-E/kT), \qquad (10)$$

where A is the preexponential factor, k is Boltzmann's constant, T is the absolute temperature, and E is the activation energy. With the application of Eq. (10), the hopping energy for undoped $LaMnO_3$ under oxidizing conditions was calculated to be 18.3 ± 1 kJ/mole (0.19 ± 0.01 eV) which is lower than the 24 kJ/mole (0.25 eV) reported by Goodenough (*11*). Since $LaMnO_3$ possesses different Mn^{+4} content depending upon the preparation conditions, this small difference in activation energy is understandable. Hopping energies were calculated as 18.3 ± 1, 15.4 ± 1, 8.7 ± 1 kJ/mole (0.19 ± 0.01, 0.16 ± 0.01, and 0.09 ± 0.01 eV) for 5, 10, and 20 mol% Sr-doped $LaMnO_3$, respectively.

B. Seebeck Coefficient

Since the electrical conductivity data clearly indicated that carriers moved via the small polaron hopping mechanism, the Heikes formula (*2*) (Eq. (11)) was used to interpret the Seebeck data. By using the assumption that only one polaron is allowed on a given site and that both spin and orbital degeneracy are negligible, Heikes derived

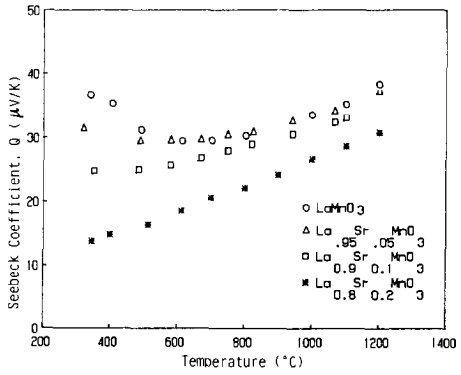

FIG. 6. Seebeck coefficient vs temperature for undoped and Sr-doped $LaMnO_3$.

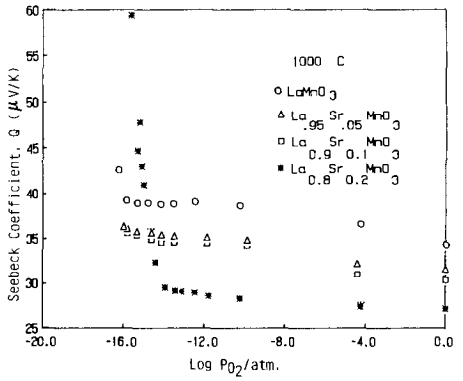

FIG. 7. Seebeck coefficient vs log P_{O_2} for undoped and Sr-doped $LaMnO_3$ at 1000°C.

the following relationship for the Seebeck coefficient,

$$Q = \pm(k/e)[\ln((1 - x)/x) + S^*/k], \quad (11)$$

where the plus and minus signs indicate p-type and n-type carriers, respectively, k is the Boltzmann constant, x is the fraction of hopping sites which are occupied, and S^* is the vibrational entropy. When S^* is assumed small enough to be negligible, the Seebeck coefficient depends only on the concentration term. This equation leads to a temperature-independent Seebeck coefficient for degenerate polaron energies. The Seebeck coefficients for undoped $LaMnO_3$ and 5, 10, and 20 mol% Sr-doped $LaMnO_3$ were measured as a function of temperature with the results shown in Fig. 6. The positive Seebeck coefficients indicate that these oxides are p-type. The variation of Q for these (La, Sr)MnO_3 samples in the temperature range investigated is relatively weak when compared with that observed for other lanthanum perovskites such as $LaCrO_3$ (*12*) and (La, Sr)FeO_3 (*13, 14*). According to Eq. (11), the weak temperature dependence of Q implies that the carrier concentration is nearly temperature independent. Therefore, the observed temperature dependence of electrical conductivity would depend largely on mobility.

Seebeck measurements were made as a function of P_{O_2} and temperature. Typical results for undoped $LaMnO_3$ and 5, 10, and 20 mol% Sr-doped $LaMnO_3$ are shown in Fig. 7. With decreasing P_{O_2}, the Seebeck coefficient increased to a maximum after which it became negative. These negative values are not included in Fig. 7. The P_{O_2} at which the Seebeck coefficient changed from positive to negative compared with the "critical P_{O_2}" observed in the TG and electrical conductivity data. This sign reversal may be due to the decomposition of the perovskite phase. Figure 8 shows a typical rela-

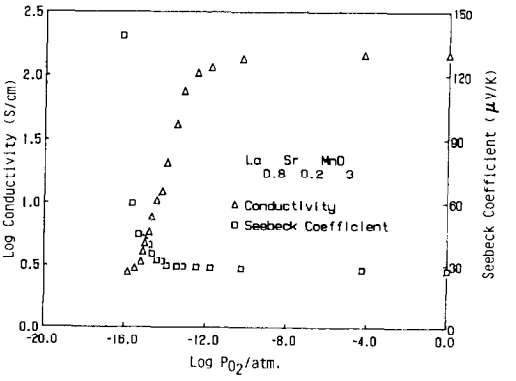

FIG. 8. Seebeck coefficient and log conductivity (dc) vs log P_{O_2} for $La_{.80}Sr_{.20}MnO_3$ at 1000°C, respectively.

tionship between electrical conductivity and Seebeck coefficient for 20 mol% Sr-doped $LaMnO_3$ at 1000°C. Note that the equivalent TG critical P_{O_2} for the same material was found to be 10^{-16} atm (*1*).

By using Eq. (11) and by assuming that the entropy S^* is negligible, the fraction of sites occupied at 1000°C in an oxygen atmosphere was calculated to be 0.39 and 0.41 for undoped and 20 mol% Sr-doped $LaMnO_3$, respectively. These calculated fractions of hopping sites are clearly too high to result from doping alone. In addition the absolute values of the measured Seebeck coefficients in (La, Sr)MnO_3 systems are smaller than the 100 μV/K criterion suggested by Goodenough (*15*) for the small polaron mechanism. Similar behavior has been reported in the $La_{1-y}Sr_yCoO_{3-x}$ system (*16*). This may indicate that the conduction mechanism is more complicated than that proposed by Heikes in that another source of carriers may be involved in the transport mechanism. For example, carriers originating from the band to band transition may be contributing to the conduction at elevated temperatures. Analogous to the (La, Sr)CoO_3 system, at elevated temperatures (La, Sr)MnO_3 may have a conduction mechanism intermediate between a metal and semiconductor.

C. Mobility

The mobility was determined by combining the Seebeck and electrical conductivity data. Since the Seebeck coefficients were positive until decomposition occurred, the electrical conductivity is assumed to be due to holes. The hole electrical conductivity is given by

$$\sigma = (A_v/V_M)pe\mu, \qquad (12)$$

where A_v is Avogadro's number, V_M is the molar volume, p is the molar fraction of holes, e is the unit charge, and μ is the hole mobility. The Seebeck coefficient for holes can be represented by

$$Q = (k/e)[\ln(N_v V_M/A_v p)], \qquad (13)$$

where k is Boltzmann's constant and N_v is the density of states. As for Eq. (11), it is assumed in Eq. (13) that the S^* term is small enough to be neglected and that the states of the semiconductor are nondegenerate. When Eqs. (12) and (13) are combined, the following equation for Q results

$$Q = (k/e)\ln(N_v e\mu/\sigma). \qquad (14)$$

Rearranging, the mobility becomes

$$\mu = (\sigma/N_v e)\exp(Qe/k). \qquad (15)$$

By assuming cubic symmetry (*17*) and a lattice parameter for undoped $LaMnO_3$ of 3.88 A, the density of states N_v can be calculated as 1.712×10^{22} cm^{-3}. By using this value for the density of states and the experimental Q and σ data, the mobility for undoped $LaMnO_3$ was calculated from Eq. (15) as a function of P_{O_2} and temperature.

By assuming that the lattice parameter for 20 mol% Sr-doped $LaMnO_3$ is similar to that for undoped $LaMnO_3$, the same density of states was used. The calculated hole mobilities for undoped $LaMnO_3$ and 20 mol% Sr-doped $LaMnO_3$ are shown in Fig. 9.

We analyzed the electrical conductivity data by assuming that the mobility was inde-

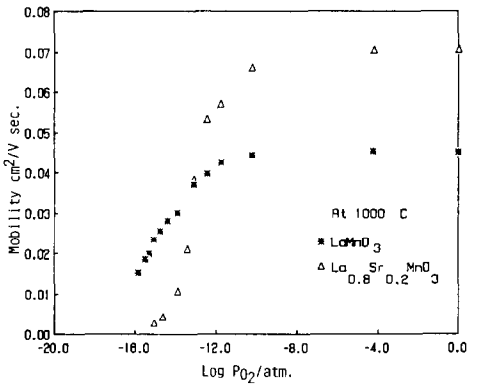

FIG. 9. Mobility vs log P_{O_2} for undoped and Sr-doped $LaMnO_3$ at 1000°C.

TABLE II

THE CORRECTED EQUILIBRIUM CONSTANTS FOR $La_{.8}Sr_{.2}MnO_3$

	1000°C	1100°C	1200°C
Log K_1' (Corrected)	−7.04	−6.52	−6.00
Log K_1 (Original)	−5.04	−4.52	−4.00
Log K_1 (TGA)	−8.68	−7.59	−6.65

pendent of P_{O_2} and that the carrier concentration in the high P_{O_2} region was equal to the doping concentrations. However, as can be seen in Fig. 9, the calculated mobilities for undoped $LaMnO_3$ and 20 mol% Sr-doped $LaMnO_3$ show both temperature and P_{O_2} dependence. Furthermore, the calculated carrier concentrations were found to be higher than the doping concentrations. Thus the expression used to analyze the electrical conductivity data needs to be altered to include the variable mobility and calculated carrier concentration. When this is done the corrected equilibrium constant becomes

$$K_1' = (\mu/\mu_R)^2(y/y')K_1, \qquad (16)$$

where K_1' represents the corrected equilibrium constant. The mobilities μ and μ_R correspond to those in the low and high P_{O_2} regions, respectively. The carrier concentration, y, is assumed to be equal to the doping concentration and y' is the calculated carrier concentration. K_1 is the original equilibrium constant calculated from Eq. (9).

By using the case of $La_{0.8}Sr_{0.2}MnO_3$ as an example, with y' equal to 0.412 and μ and μ_R estimated from Fig. 9, the corrected equilibrium constant K_1' is calculated by using Eq. (16). Table II compares the corrected equilibrium constant K_1' and the original equilibrium constant K_1 with those obtained from the previous TG study. As can be seen, the corrected equilibrium constant resulted in better agreement with the TG results.

At 1000°C the maximum mobility for undoped $LaMnO_3$ and $La_{0.8}Sr_{0.2}MnO_3$ was calculated to be 0.045 and 0.071 $cm^2 V^{-1} sec^{-1}$, respectively. These results showed that the mobility of undoped $LaMnO_3$ has appreciably increased with the addition of Sr. Since the carrier concentrations calculated from the Seebeck measurements suggested that the carrier concentration was essentially independent of Sr content, it is concluded that the electrical conductivity for these $LaMnO_3$-based perovskites is dominated by the mobility rather than by the carrier concentration.

Note that the values of mobility for $LaMnO_3$-based perovskites calculated above are only approximate, since the Heikes formula which assumed that both spin and orbital degeneracy were negligible was used in the calculation. The real situation may be more complicated than that described by the Heikes formula. However, these small mobility values are consistent with the criteria given by Goodenough (*15*).

By combining the Seebeck (Fig. 6) and dc electrical conductivity data (Fig. 5) with Eq. (15), the mobilities for undoped $LaMnO_3$ and 5, 10, and 20 mol% Sr-doped $LaMnO_3$ were calculated as a function of temperature. The results are shown in Fig. 10. These mobilities are the maxima with respect to each composition since they were measured in an oxygen atmosphere. For a small po-

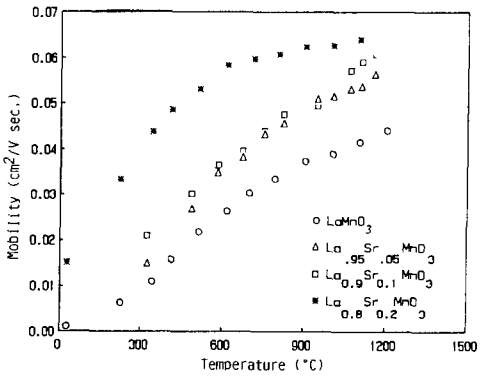

FIG. 10. Mobility vs temperature for undoped and Sr-doped $LaMnO_3$.

laron hopping mechanism, the mobility can be expressed as

$$\mu = (A/T) \exp(-W_H/kT), \quad (17)$$

where A is the preexponential factor, T is the temperature, k is Boltzmann's constant, and W_H is the hopping energy. A straight line is expected in a $\ln(\mu T)$ vs $1/T$ plot if the conduction follows the small polaron hopping mechanism. By using a least-squares method, the hopping energies were calculated as 19.3 ± 1, 18.3 ± 1, 16.4 ± 1, and 10.6 ± 1 kJ/mole (0.20 ± 0.01, 0.19 ± 0.01, 0.17 ± 0.01, and 0.11 ± 0.01 eV) for undoped $LaMnO_3$ and 5, 10, and 20 mol% Sr-doped $LaMnO_3$, respectively.

Note that, within the accuracy of the measurement, these hopping energies are the same as those calculated from the electrical conductivity data (Fig. 5) which yielded 16.4 ± 1, 16.4 ± 1, 15.4 ± 1, and 8.7 ± 1 kJ/mole (0.19 ± 0.01, 0.19 ± 0.01, 0.16 ± 0.01, and 0.09 ± 0.01 eV) for undoped $LaMnO_3$ and 5, 10, and 20 mol% Sr-doped $LaMnO_3$, respectively.

4. Conclusion

1. Electrical conductivity and Seebeck coefficient measurements show that undoped and Sr-doped $LaMnO_3$ (up to 20 mol%) are p-type. The electrical conductivity of undoped $LaMnO_3$ was enhanced by the addition of Sr. As reduction proceeded, the electrical conductivity decreases as $P_{O_2}^{1/4}$. A defect model was proposed to explain the above observation.

2. The oxidation–reduction behavior was found to be reversible. Phase stability in a reducing atmosphere was decreased by the addition of Sr. The critical P_{O_2} values determined from the electrical conductivity, the Seebeck coefficient, and the previous TG results showed good agreement.

3. The carrier concentration and the mobility were calculated from the dc electrical conductivity and the Seebeck coefficients by using the Heikes formula. The results suggest that the temperature dependence of the electrical conductivity for these $LaMnO_3$-based perovskites is dominated by the mobility rather than by the carrier concentration.

5. Acknowledgment

The authors express their appreciation for the financial support provided by the Basic Energy Science Division of the Department of Energy to carry out this study.

References

1. J. H. Kuo, H. U. Anderson, and D. M. Sparlin, *J. Solid State Chem.* **83,** 52 (1989).
2. R. R. Heikes, "Thermoelectricity," Interscience, New York (1961).
3. M. P. Pechini, "Method of Preparing Lead and Alkaline Earth Titanates and Niobates and Coating Method Using the Same to Form a Capacitor," U.S. Patent 3,330,697.
4. L. J. van der Pauw, *Philips Res. Rep.* **13,** 1, (1958).
5. H. U. Anderson, M. M. Nasrallah, B. K. Flandermeyer, and A. K. Agarwal, *J. Solid State Chem.* **56,** 325 (1985).
6. G. V. Subba Rao, B. M. Wanklyn, and C. N. R. Rao, *J. Phys. Chem. Solids* **36,** 345 (1971).
7. R. S. Roth, "Progress in Science and Technology of Rare Earths," Pergamon, Elmsford, NY (1964).
8. P. M. Raccah and J. B. Goodenough, *Phys. Rev.* **155,** 932 (1967).
9. G. Matsumoto, "Proc. Int. Conf. Ferrites, Japan, July, 1970."
10. V. I. Pavlov, A. K. Bogush, and G. L. Bychkov, *Inorg. Mater.* **20(5),** 752 (1984).
11. J. B. Goodenough, *Phys. Rev.* **100,** 564 (1953).
12. D. P. Karim and A. T. Aldred, *Phys. Rev. B* **20,** 2255 (1979).
13. J. Mizusaki, T. Sasamoto, W. R. Cannon, and H. K. Bowen, *J. Amer. Ceram. Soc.* **65,** 363 (1982).
14. J. Mizusaki, T. Sasamoto, W. R. Cannon, and H. K. Bowen, *J. Amer. Ceram. Soc.* **66,** 247 (1983).
15. J. B. Goodenough, *Prog. Solid State Chem.* **5,** 238 (1971).
16. F. R. van Buren and J. H. W. de Wit, *J. Electrochem. Soc.* **126,** 1817 (1979).
17. Naray-Szabo, *Naturwissenschaften* **31,** 466 (1943).